JACS
JOURNAL OF THE AMERICAN CHEMICAL SOCIETY
Article
Cite This: J. Am. Chem. Soc. 2018, 140, 14670−14676
pubs.acs.org/JACS

Layered-Crossover Tiles with Precisely Tunable Angles for 2D and 3D DNA Crystal Engineering

Fan Hong, Shuoxing Jiang, Xiang Lan, Raghu Pradeep Narayanan, Petr Šulc, Fei Zhang,* Yan Liu,* and Hao Yan*

Center for Molecular Design and Biomimetics at the Biodesign Institute and School of Molecular Sciences, Arizona State University, Tempe, Arizona 85287, United States

Supporting Information

ABSTRACT: DNA tile-based assembly provides a promising bottom-up avenue to create designer two-dimensional (2D) and three-dimensional (3D) crystalline structures that may host guest molecules or nanoparticles to achieve novel functionalities. Herein, we introduce a new kind of DNA tiles (named layered-crossover tiles) that each consists of two or four pairs of layered crossovers to bridge DNA helices in two neighboring layers with precisely predetermined relative orientations. By providing proper matching rules for the sticky ends at the terminals, these layered-crossover tiles are able to assemble into 2D periodic lattices with precisely controlled angles ranging from 20° to 80°. The layered-crossover tile can be slightly modified and used to successfully assemble 3D lattice with dimensions of several hundred micrometers with tunable angles as well. These layered-crossover tiles significantly expand the toolbox of DNA nanotechnology to construct materials through bottom-up approaches.

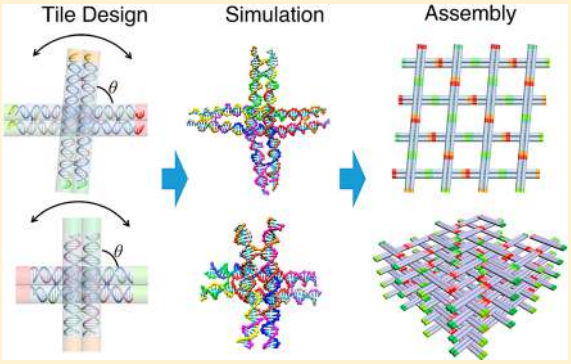

INTRODUCTION

The programmability of DNA enables the bottom-up construction of designer molecular structures that can be widely used in nanorobotics, nanophotonics, smart drug deliveries, templated material synthesis, and so on.[1−5] Generally, the assembly of DNA nanostructures uses one of the two main methods, DNA origami-based or DNA tile-based self-assembly. For DNA origami, a long scaffold strand is used to assist the assembly of hundreds of shorter strands (15−60-nt) into a predetermined shape.[6−15] Recently, the design of single-stranded DNA origami has also been reported that a single-stranded DNA is able to fold itself to form designer structures up to 10,000 nucleotides.[16] In a tile-based assembly, the shorter strands generally will first assemble into unique or identical unit tiles, which then further assemble into higher ordered finite structures with well-defined boundaries[17−20] or infinite two-dimensional (2D) tessellations and three-dimensional (3D) crystals.[21−28] Using DNA tiles for 2D tessellation attracts lots of interest because the programmability of DNA enables a variety of mathematic tessellations in nanoscale, which may lead to the discovery and construction of novel materials. For example, using a single type of regular polygons (such as squares, equilateral triangles, and regular hexagons) to tessellate a plane, referred as regular tessellations, has been achieved by using various symmetric multiple-arm junction DNA tiles.[21,23,24] To create more complicated 2D patterns other than regular tessellations, such as Archimedean tessellations,[29] the symmetry of the assembly tile units need to be reduced. There are two ways to reduce the assembly symmetry, one is to use multiple tiles with various geometries,[30] and another one is to break down the symmetry of a single tile.[31,32] It is also possible to further reduce the assembly symmetry to create even more complicated quasicrystal patterns. The 3D crystals with predefined geometry can be implemented to host guest molecules to construct new materials from bottom-up approaches[33,34] and possibly to scaffold proteins for structure determination.[35]

DESIGN

To engineer more diverse and complicated 2D and 3D crystal patterns, new DNA motifs and assembly strategies need to be invented. The layered-crossover motif, which is a derivative from the traditional double crossover DNA motif,[36] has been previously used to construct 3D framework DNA origami structures.[37] Herein, we implemented the layered-crossover motif to construct a set of rhombus-like layered-crossover DNA tiles with precisely tunable orientation angles to achieve nonregular tessellations. Moreover, the layered-crossover tile can also be designed to assemble into 3D crystals with dimensions up to hundreds of micrometers.

The rhombus DNA tile with layered-crossovers is composed of two double crossover DNA molecules that are laid in two layers with a predetermined angle (Figure 1 and Figure S1).

Received: July 7, 2018
Published: October 18, 2018

DOI: 10.1021/jacs.8b07180
J. Am. Chem. Soc. 2018, 140, 14670−14676

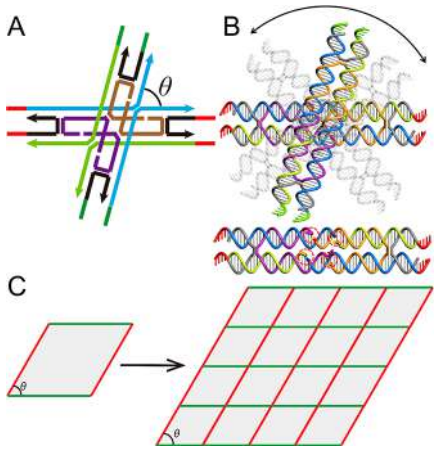

Figure 1. Design of layered-crossover tile for nonregular tessellations. (A, B) The line and helical models of the layered-crossover tile. In (B) the model at the bottom shows the top view after the helices in the top layer are cut off that reveals the four layered crossover points indicated in red circles. Different combinations of the crossover points can be selected to connect the DNA helices in two layers, which will precisely tune the angle θ between the layered helices. (C) A scheme of tessellation with an abstracted rhombus tile of angle θ.

Unlike the traditional double crossovers that hold DNA helices in parallel style in the same plane (two of such crossovers are visible in Figure 1B, the cutoff view), the layered-crossovers are able to allow nonparallel alignment of DNA helices between layers and create the 3D interaction with a defined geometry. The relative orientation between DNA helices in neighboring layers can be precisely controlled through the combination of different available layered-crossovers along the DNA helices (Figures S2–S4). By taking the advantage of this property, we first constructed a set of two-layered DNA tiles with many defined angles to fill 2D space with intended angles of approximately 90°, 75°, 60°, 45°, 30°, and 20°.

To design a layered-crossover tile, the key is to find the optimal positions to create a crossover pair between the layers to immobilize the orientation of the DNA helices. Similar to the traditional double crossover that has the smallest distance between the parallel DNA helices, the layered-crossovers would give the closest distance between layers of DNA helices as well. Consequently, the position to create a layered-crossover should be located at the top or bottom of the DNA helices. When the DNA helices have been aligned with a desired angle, a layered-crossover can be created to allow a DNA strand to travel between layers through the backbone of the closest bases between layered helices, which fixes the orientation angle (Figure S5). Based on the rules above, we used the Tiamat software to design a set of layered-crossover tiles with various angles by using the different combination of layered-crossover pairs. The strand pathways of each tile were shown in Figure 2A.

RESULTS AND DISCUSSION

To gain insight and quantitative analysis of the designed tiles, coarse-grained molecular dynamics simulations were performed using oxDNA. The oxDNA model is a coarse-grained DNA model that captures the structural, thermodynamic, and

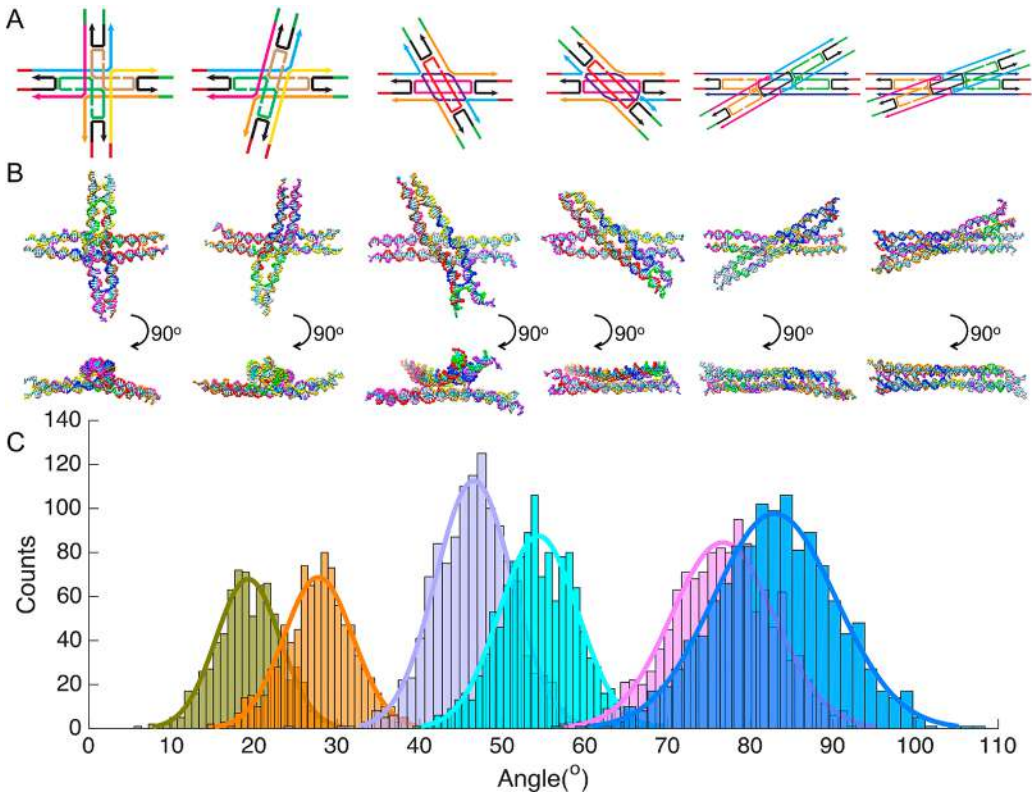

Figure 2. Simulation of the layered-crossover tiles with coarse-grained oxDNA model. (A) Line model and (B) top and side views of typical configurations from oxDNA simulations of the layered-crossover tile with different orientation angles, in a decreasing order of the acute angle. (C) Histograms of angle distribution of the layered-crossover tiles from simulations. The mean angles are determined to be 83 ± 7°, 76 ± 6°, 55 ± 5°, 45 ± 5°, 28 ± 4°, and 20 ± 4°, respectively.

DOI: 10.1021/jacs.8b07180
J. Am. Chem. Soc. 2018, 140, 14670–14676

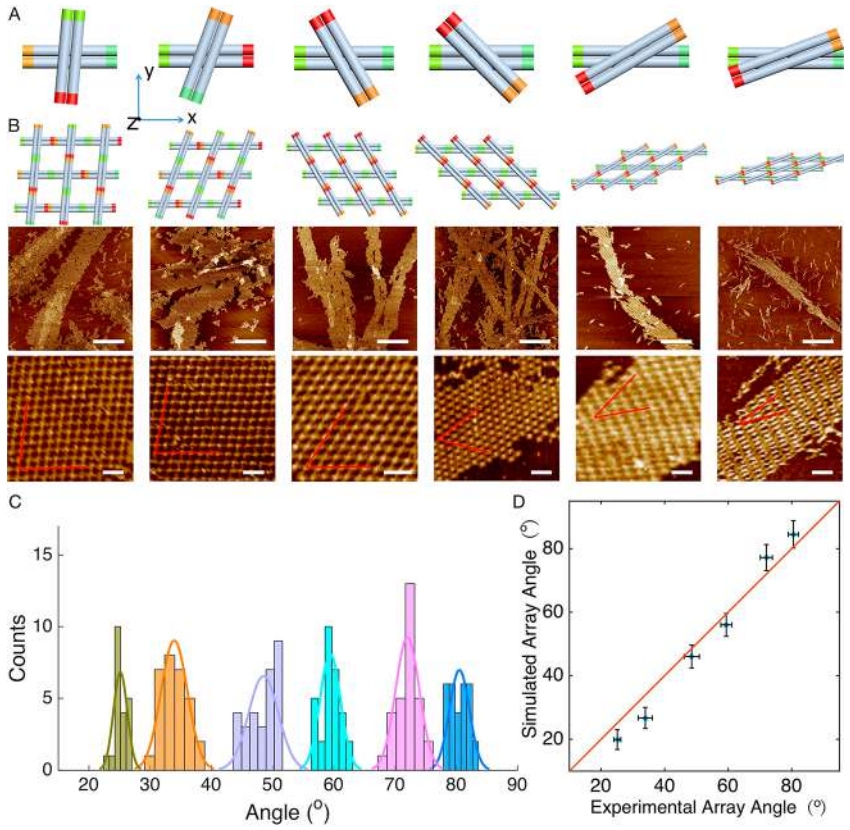

Figure 3. 2D tessellation by the layered-crossover tiles with predefined orientation angles. The colors of the sticky ends represent the matching properties: red matches orange and light green matches green. (A) Cylinder models of the layered-crossover tile with different orientation angles, in a decreasing order of the acute angle. (B) The cylinder model and AFM images of 2D array patterns assembled by the corresponding layered-crossover tiles. The scale bars in the top and bottom AFM images are 500 and 50 nm, respectively. (C) Histograms of angle distribution of the 2D crystals measured from the AFM images. The corresponding solid lines represent the single peak Gaussian fitting curves of the distributions of the angle of tile lattice. The mean angles are determined to be 81 ± 2° (n = 32), 73 ± 2° (n = 32), 59 ± 2° (n = 32), 49 ± 2° (n = 32), 34 ± 2° (n = 32), 25 ± 1° (n = 28). The angle of each scenarios is measured as the acute angle, by randomly selecting a number of 6 × 6 lattices. (D) The plot of the predicted angles by coarse-grained model versus the experimentally measured angles from AFM images.

mechanical properties of both single-stranded DNA and double-stranded DNA, which has been previously used to characterize a range of DNA nanostructures and active devices.[38,39] The orientation angle of the DNA tiles in the simulation was measured by the angle between the vector connecting the double crossovers in the top layer and the vector connecting the double crossovers in the bottom layer (Figure S6). Snapshots of the simulated DNA tile conformations are shown in Figure 2B (more design and simulation details of the structure can be found in Figures S7−S19). The angle distributions of the six simulated designs are shown in Figure 2C, which are 83 ± 7°, 76 ± 6°, 55 ± 5°, 45 ± 5°, 28 ± 4°, and 20 ± 4°, respectively.

We hypothesized that the 2D lattice formed by these tiles would have a smaller angle variance due to constrains from binding of neighboring tiles. To verify the assumption, we simulated a small 3 × 3 lattice using oxDNA using the different tiles and measured the angles to be 84 ± 4°, 77 ± 4°, 56 ± 4°, 46 ± 4°, 27 ± 3°, and 20 ± 3°, respectively, which indeed showed a significant decrease of the angle variance (Figures S20−S27).

We then move to the experimental validation of the designs. Considering the layered-crossover tile with a predicted angle of 83° as an example (Figure 3A), as the layered-crossover DNA motif might have a certain degree of curvature, both corrugated and noncorrugated designs have been attempted to assemble the 2D crystal. The assembly of single tile unit and high-order structure by the tile have been verified by native gel electrophoresis (Figure S28). The corrugated assembly strategy used a single tile and considered the two-layered structure that is geometrically different from that of the traditional single-layered tiles.[21] For a single type of tile to assemble together in a corrugated manner, the neighboring tiles have to flip 180° along y-axis and then rotate around z-axis about 83° to match the paring rule (Figure S29). Figure 3B (first row from the top and Figure S30) shows AFM images demonstrating the 2D periodic patterns from the corrugated design (results from noncorrugated designs can be found in Figure S31). No significant difference between the corrugated and noncorrugated designs was found (Figure S32). The angle of a number (>20) of 6 × 6 lattices on AFM images was measured to be 81 ± 2 (mean ± SD) with the corrugated design tiles, which has a narrower distribution and matches well with the calculated angle from the coarse-grain model simulation.

We further experimentally tested the tessellation of the rest of tiles with the model simulated angles of 76°, 55°, 45°, 28°, and 20°. Since no difference was found between the corrugated and noncorrugated designs, the assembly of the 76° tile employed the corrugated connection strategy, and the others used the noncorrugated assembly design. It is noted that the smaller the angle between the layered DNA helices is, a longer

DOI: 10.1021/jacs.8b07180
J. Am. Chem. Soc. 2018, 140, 14670−14676

distance between the pair of layered crossovers is required. The length of the overall helices of 28° and 20° tiles was therefore extended by one DNA helical turn to adopt a longer distance between the layered-crossover pairs. All the tiles are able to grow into 2D tessellated plane (Figure 3B, additional AFM images are shown in Figures S33−S37). The measured angles of the helices in the 2D lattices are 73 ± 2°, 59 ± 2°, 49 ± 2°, 34 ± 2°, and 25 ± 1°, respectively (Figure 3C), matching the model prediction very well (Figure 3D). The angles calculated from the simulated conformation and angles measured from the AFM images are all close to the intended angle during the design based on a simple geometric consideration. The coarse-grain model was able to give reasonable information to the design of layered-crossover tile prior to experimental trials. The small discrepancy between the experimental value and the model predicted value of the lattice angle may be attributed to possible inaccuracies of the structure representation in the model due to its coarse-grained nature, as well as the AFM imaging conditions used in the experiment. During AFM imaging, all the lattices are forced to attached to the mica surface, which may cause expansion of the angles especially for those with smaller angles. In addition, the ion bridge between the DNA lattice and mica constrains the DNA lattice movement, which narrows the angle distribution.

We also observed tube formation in all assemblies of the designed tiles under AFM (in the mixture of small stripes of 2D arrays). Tube formation is a common phenomenon in the DNA tile-based self-assembly.[40] When the tiles grow into larger patches of 2D lattices, and the enthalpy gain through pairing the edge sticky ends is able to compensate the entropy loss of the tube closing, the lattice would tend to curl and close up into tube structures to minimize the free energy of the system. It is interesting to note that comparing the tubes formed by the 83° tile with the tubes formed by the 55° tile, the former consistently have a larger tube diameter (Figure S38). Two factors may contribute to the difference. One is the difference between the tile's intrinsic flexibility and curvature, which is difficult to quantify experimentally. The second is the difference between the orientation angles of the unit tiles. To fold a sheet of 2D array of the same dimension into a tube, for the tile array with a smaller angle, more edge offset is shifted to accommodate the sticky end's association, which results in a smaller diameter (Figure S39).

Surface substrates, such as mica[41,42] and lipid bilayer,[43−45] have been previously explored to aid the assembly of DNA nanostructures in 2D to reduce the effect of flexibility and intrinsic curvature of the tile. We hypothesized that the electrostatic interactions between the DNA tile and the mica surface would confine the tile's assembly on the 2D surface thus prevent tube formation (Figure 4A). To achieve a successful 2D lattice assembly supported on the mica surface, the tile concentration should be optimized to avoid over-crowding or too low material coverage. Using a wide range of concentrations for the assembly (Figure S40), we found that approximately 40 μL of 5 nM (200 femtomole) of DNA tile (76° tile) could cover the whole surface (mica disc, diameter of 10 mm) with nearly 100% coverage (Figure 4B−D), while the tile concentration required in solution-based assembly usually is at 100 μL of 1 μM (100 pmole) scale. Additional AFM images for the tiles with other angles are shown in Figures S41−43. No tubes were observed under the condition of the mica surface-mediated assembly. Defects included miss-matched tiles at the domain boundaries, and a tile or two

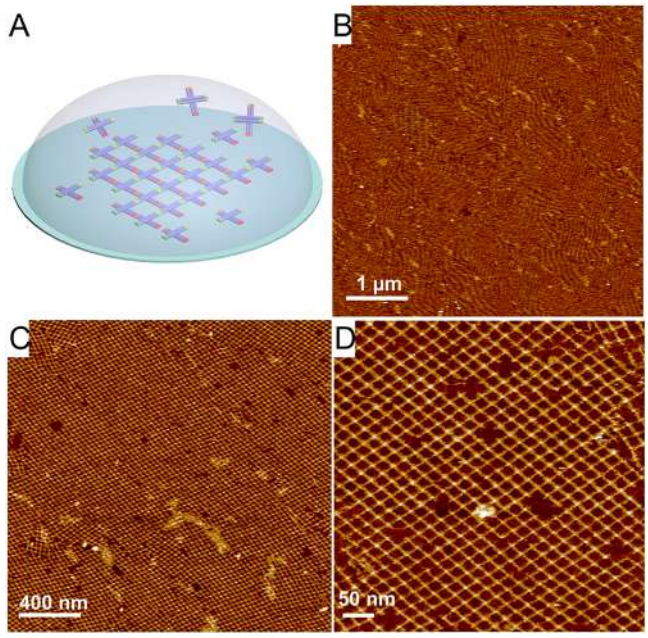

Figure 4. Surface-mediated assembly of the layered-crossover tile with 76° tiles. (A) The scheme of the surface-mediated assembly. Ideally, after the nucleus is formed, the tile will attach to the nucleus either directly from solution to the mica surface or diffuse on the surface and reorientate itself before attaching to the growing front of a lattice. (B−D) AFM images of the 2D crystal on mica surface in different scan scales. In (B) the whole mica surface is almost fully covered by a single layer of DNA 2D crystals (with domain sizes ∼200 nm to several microns). In (C) and (D) the missing tile defects are likely caused by scratching the AFM tips as subsequent imaging of the same area shows more defects. Domain boundary defects are also visible reflecting that the different domains are grown separately from different nuclei on the surface until they touch one another.

missing in the middle of the domains, which are related to the nucleation and growth rates on the surface and damages by the scanning AFM tip, respectively.

We further tried to extend the growth of layered-crossover tiles to 3D crystal engineering. Although it seems straightforward to simply extend the current 2D design to a 3D growth, the experimental assembly conditions of 2D and 3D crystals are quite different, thus some structural modifications are necessary to make the assembly successful. Generally, in a 3D crystallization setup, a relatively high concentration of DNA units (100−300 μM) is required to form micrometer-sized crystals. This concentration is orders of magnitude higher than that used in the 2D assembly. This high concentration requires that the interactions between the units should remain very weak to avoid too fast nucleation, which may result in many tiny crystals rather than a few big crystals. In addition, the topology of the strands in the unit should be as simple as possible to avoid undesired interactions that cause irreversible aggregations and kinetic traps.

The tile units for 2D lattice consist of 12 different strands including some long strands (>60 nucleotides) and relatively complex routing topology because of the four layered-crossovers. Therefore, they are more prone to have errors both in terms of stoichiometry and sequence pairing under the 3D crystal assembly conditions. To reduce the number of strands and topological complexities in the unit, a pair of layer-crossover points were removed, and a symmetry design rule was applied, so that only five strands were used (Figure 5A and

DOI: 10.1021/jacs.8b07180
J. Am. Chem. Soc. 2018, 140, 14670−14676

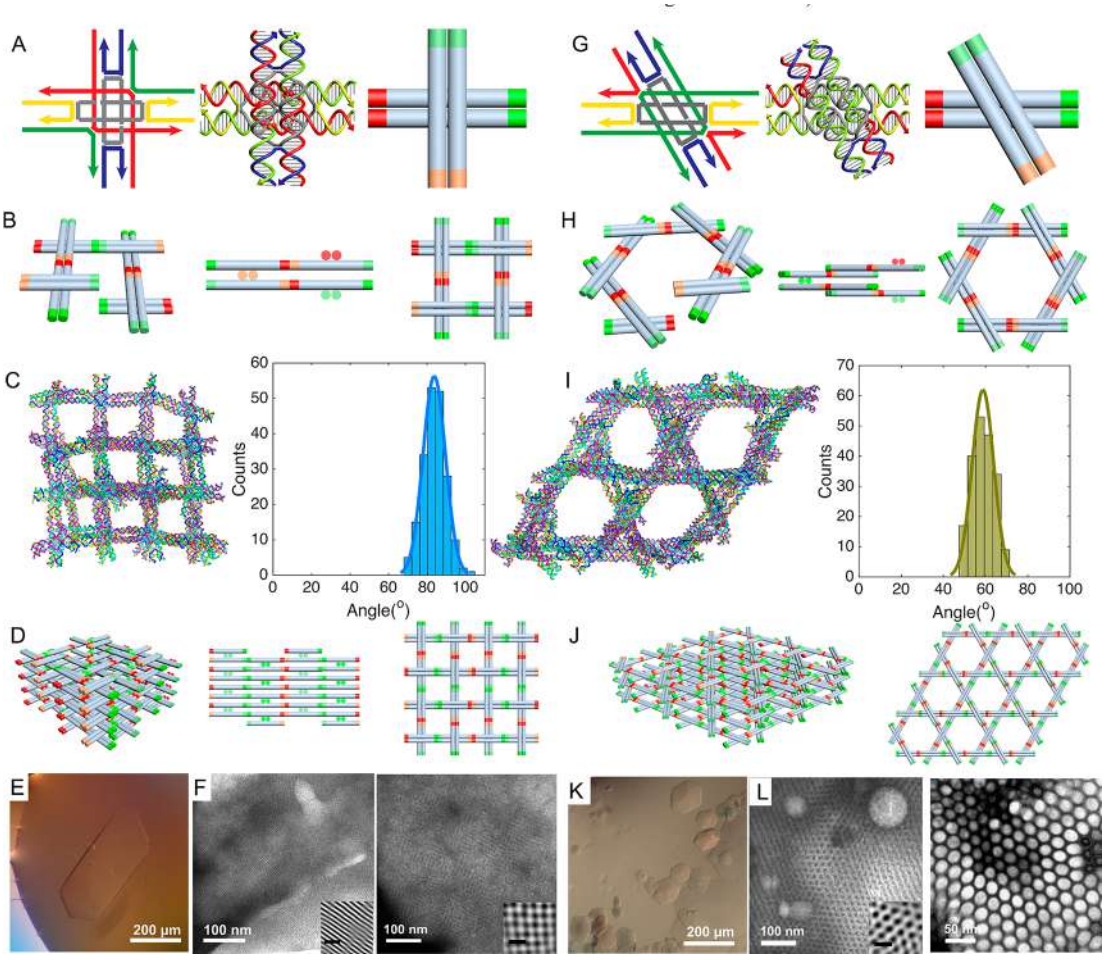

Figure 5. 3D crystals assembled from layered-crossover tiles with two different angles, 90° and 60°, respectively. (A, G) Line, helical, and cylinder models of the layered-crossover tiles. (B, H) The assemble rule of the layered-crossover tiles into 3D crystal. The colors of the sticky ends represent the matching rules: red matches orange and light green matches green. To match the encoded interaction rules, the tiles need to rotate a certain degree (90° in B, and 60° in H) and then shift one helix layer up or down, leading to 3D growth. (C, I) Snapshots of the conformation of the simulated crystal assembly and the calculated angle distribution for the square and hexagonal design, respectively. The solid lines represent the single peak Gaussian fitting curves of the distributions of the angle of layered-crossover tile. The mean angles are determined to be 84 ± 5° and 59 ± 5°, respectively. (D, J) The assembled 3D DNA crystal model projections from different perspectives. (E, K) The assembled 3D crystal images taken by optical microscope under polarized light. (F, L) TEM images of the 3D crystal assembled. The inserts in (F, L) are the reconstructed images from FFT (black scale bars are 20 nm).

G). In addition, the sticky ends were reduced in length to weaken the interactions, and the arm lengths were also reduced to avoid long strands.

For a tile with an orientation angle θ, to adopt a 3D growth, the tile needs to rotate angle θ and then shift one helix layer up or down to match the paring rule. Consequently, the pattern of the assembled 3D crystal will depend on the orientation angle of the layered-crossover tiles. For a proof of concept, we designed two layered-crossover tiles with different orientation angles, 90° and 60°, respectively. All the sticky ends are 1-nt long, and each arm is shortened by one helical turn. To match the sticky ends of one unit, the neighboring units were designed to rotate their orientation angles either 90° or 60° in plane with respect to that unit and then shift one helix (Figure 5B,H, Figure S44) layer up or down, leading to a 3D growth. Based on such defined matching rules, the final crystals are expected to have a four-fold and six-fold helical symmetry that have square or hexagonal repeating patterns from the top view, respectively (the detail of the designed tiles are shown in Figures S45 and S46).

With these symmetries, the angles of the tiles in the crystals are assumed to be 90° or 60° for an extended 3D crystal to be able to form, respectively. The simulated structures and angle calculations (84 ± 5° and 59 ± 5°, respectively) of tile in the crystal assembly based on the oxDNA model are shown in Figure 5C,I. The angle distributions of the free tile (74 ± 9° and 52 ± 5°, respectively) are also simulated and shown in Figures S47 and S48. The wider angle distributions of the free tiles compared with that of the tiles used for the 2D growth may be because of the 2-point contact used here instead of 4-point contact between the two layers.

The formation of the unit was checked by native gel electrophoresis (Figure S49). Observed using optical microscopy under polarized light, the assembled crystals from the two designs both have a thin sheet morphology with $x-y$ dimensions up to several hundred micrometers (Figure 5E,K). Additional crystal images can be found in Figures S50 and S51. We gently broke the selected crystals harvested from the crystallization buffer into smaller pieces and applied negative staining to observe the crystalline structural pattern by

DOI: 10.1021/jacs.8b07180
J. Am. Chem. Soc. 2018, 140, 14670−14676

TEM. For the square design, the TEM images from two different projections are shown in Figure 5F,L (additional TEM images can be found in Figures S52–S53), from which we observed the parallel lines and square grid patterns, respectively. The images reconstructed from Fast fourier transform (FFT) of the TEM images indicate that the distance between the parallel lines in the side view and the dimensions of the cavities from the top view are about 4.3 ± 0.2 nm and 11.9 ± 0.4 nm, respectively, which match with the designed crystals based on the dimensions of the DNA tiles (two layers of DNA helices and four full helical turns). For the hexagonal design, only the hexagonal pattern from top view was observed. The side length of the hexagonal cavity is measured to be about 14.9 ± 1.1 nm in TEM images, while the designed length is 15.3 nm (the calculation of the designed length is shown in Figure S54). The angles of the cavity of the two assembled crystals in the TEM images are measured to be 85 ± 3° and 59 ± 5°, respectively, slightly deviated from the expected 90° or 60°, which may be likely due to the incident angle of the electron beam in the TEM imaging not being perfectly parallel with the symmetry axis of the crystal being analyzed.

The design of square 3D crystal unit was also tried for 2D assembly by increasing the sticky end length and changing the paring rule, but no 2D lattice was successfully assembled, indicating that the simplified 3D design may not be suitable for 2D assembly (Figure S55). The reason may be that the strong interactions between the tiles at the ends of the helices may distort the crossovers from their desired alignment (detailed discussions can be found in the Section 7 of the Supporting Information).

CONCLUSIONS

In summary, we have demonstrated a new DNA tile motif that can be applied to construct both 2D and 3D DNA crystals. Unlike previous multiarm junction tiles, the layered-crossover tiles presented here provide a new control parameter, the orientation angles between helices, which result the tile-based self-assembly with precise lattice angle controls in both 2D and 3D. The periodic rhombic lattices with tunable angles can provide a new platform for molecule or nanoparticle organization to achieve novel properties. For example, the intercept angle between two nanorods have been proved to have great influence on their interaction with circularly polarized light.[46,47] It is possible to implement the angle-controlled lattice to organize gold nanorods in periodic arrays to achieve devices that may extensively enhance the light tailoring capability. Moreover, the 3D crystals constructed from the layered-crossover tile are in a dimension of several hundred micrometers. They can act as host materials to organize objects from molecular scale to macroscopic scale. The layered-crossover tiles enrich both the structural diversity and functionality of DNA nanostructures.

ASSOCIATED CONTENT

Supporting Information

The Supporting Information is available free of charge on the ACS Publications website at DOI: 10.1021/jacs.8b07180.

Design details of the layered-crossover tile, coarse-grain simulation results, additional AFM and TEM images of the DNA assemblies, discussions, and sequences of DNA strands (PDF)

AUTHOR INFORMATION

Corresponding Authors

*fei.zhang@asu.edu
*yan_liu@asu.edu
*hao.yan@asu.edu

ORCID

Fan Hong: 0000-0002-3370-7833
Shuoxing Jiang: 0000-0002-9235-6447
Xiang Lan: 0000-0003-4845-9956
Yan Liu: 0000-0003-0906-2606
Hao Yan: 0000-0001-7397-9852

Notes

The authors declare no competing financial interest.

ACKNOWLEDGMENTS

This work was supported by grants from National Science Foundation to H.Y. and Y.L.

REFERENCES

(1) Seeman, N. C. *Nature* **2003**, *421* (6921), 427–432.
(2) Hong, F.; Zhang, F.; Liu, Y.; Yan, H. *Chem. Rev.* **2017**, *117* (20), 12584–12640.
(3) Liu, N.; Liedl, T. *Chem. Rev.* **2018**, *118* (6), 3032–3053.
(4) Hu, Q.; Li, H.; Wang, L.; Gu, H.; Fan, C. *Chem. Rev.* **2018**, DOI: 10.1021/acs.chemrev.7b00663.
(5) Jones, M. R.; Seeman, N. C.; Mirkin, C. A. *Science* **2015**, *347* (6224), 1260901.
(6) Rothemund, P. W. *Nature* **2006**, *440* (7082), 297–302.
(7) Dietz, H.; Douglas, S. M.; Shih, W. M. *Science* **2009**, *325* (5941), 725–730.
(8) Douglas, S. M.; Dietz, H.; Liedl, T.; Hogberg, B.; Graf, F.; Shih, W. M. *Nature* **2009**, *459* (7245), 414.
(9) Han, D.; Pal, S.; Nangreave, J.; Deng, Z.; Liu, Y.; Yan, H. *Science* **2011**, *332* (6027), 342–346.
(10) Zhang, F.; Jiang, S.; Wu, S.; Li, Y.; Mao, C.; Liu, Y.; Yan, H. *Nat. Nanotechnol.* **2015**, *10* (9), 779–784.
(11) Veneziano, R.; Ratanalert, S.; Zhang, K.; Zhang, F.; Yan, H.; Chiu, W.; Bathe, M. *Science* **2016**, *352* (6293), 1534–1534.
(12) Benson, E.; Mohammed, A.; Gardell, J.; Masich, S.; Czeizler, E.; Orponen, P.; Hogberg, B. *Nature* **2015**, *523* (7561), 441–444.
(13) Castro, C. E.; Kilchherr, F.; Kim, D.-N.; Shiao, E. L.; Wauer, T.; Wortmann, P.; Bathe, M.; Dietz, H. *Nat. Methods* **2011**, *8* (3), 221.
(14) Andersen, E. S.; Dong, M.; Nielsen, M. M.; Jahn, K.; Subramani, R.; Mamdouh, W.; Golas, M. M.; Sander, B.; Stark, H.; Oliveira, C. L.; et al. *Nature* **2009**, *459* (7243), 73.
(15) Rothemund, P. W. *Nature* **2006**, *440* (7082), 297.
(16) Han, D.; Qi, X.; Myhrvold, C.; Wang, B.; Dai, M.; Jiang, S.; Bates, M.; Liu, Y.; An, B.; Zhang, F.; Yan, H.; Yin, P. *Science* **2017**, *358* (6369), eaao2648.
(17) Ke, Y.; Ong, L. L.; Shih, W. M.; Yin, P. *Science* **2012**, *338* (6111), 1177–1183.
(18) Wei, B.; Dai, M.; Yin, P. *Nature* **2012**, *485* (7400), 623.
(19) Yang, D.; Tan, Z.; Mi, Y.; Wei, B. *Nucleic Acids Res.* **2017**, *45* (6), 3606–3611.
(20) Wang, W.; Lin, T.; Zhang, S.; Bai, T.; Mi, Y.; Wei, B. *Nucleic Acids Res.* **2016**, *44* (16), 7989–7996.
(21) Yan, H.; Park, S. H.; Finkelstein, G.; Reif, J. H.; LaBean, T. H. *Science* **2003**, *301* (5641), 1882–1884.
(22) Winfree, E.; Liu, F.; Wenzler, L. A.; Seeman, N. C. *Nature* **1998**, *394* (6693), 539.
(23) He, Y.; Chen, Y.; Liu, H.; Ribbe, A. E.; Mao, C. *J. Am. Chem. Soc.* **2005**, *127* (35), 12202–12203.
(24) He, Y.; Tian, Y.; Ribbe, A. E.; Mao, C. *J. Am. Chem. Soc.* **2006**, *128* (50), 15978–15979.
(25) Ding, B.; Sha, R.; Seeman, N. C. *J. Am. Chem. Soc.* **2004**, *126* (33), 10230–10231.

(26) Zheng, J.; Birktoft, J. J.; Chen, Y.; Wang, T.; Sha, R.; Constantinou, P. E.; Ginell, S. L.; Mao, C.; Seeman, N. C. *Nature* **2009**, *461* (7260), 74.
(27) Ke, Y.; Ong, L. L.; Sun, W.; Song, J.; Dong, M.; Shih, W. M.; Yin, P. *Nat. Chem.* **2014**, *6* (11), 994−1002.
(28) Simmons, C. R.; Zhang, F.; Birktoft, J. J.; Qi, X.; Han, D.; Liu, Y.; Sha, R.; Abdallah, H. O.; Hernandez, C.; Ohayon, Y. P.; et al. *J. Am. Chem. Soc.* **2016**, *138* (31), 10047−10054.
(29) Chavey, D. *Computers & Mathematics with Applications* **1989**, *17* (1−3), 147−165.
(30) Zhang, F.; Liu, Y.; Yan, H. *J. Am. Chem. Soc.* **2013**, *135* (20), 7458−7461.
(31) Zhang, F.; Jiang, S.; Li, W.; Hunt, A.; Liu, Y.; Yan, H. *Angew. Chem.* **2016**, *128* (31), 9006−9009.
(32) Wang, P.; Wu, S.; Tian, C.; Yu, G.; Jiang, W.; Wang, G.; Mao, C. *J. Am. Chem. Soc.* **2016**, *138* (41), 13579−13585.
(33) Wang, X.; Sha, R.; Kristiansen, M.; Hernandez, C.; Hao, Y.; Mao, C.; Canary, J. W.; Seeman, N. C. *Angew. Chem.* **2017**, *129* (23), 6545−6548.
(34) Hao, Y.; Kristiansen, M.; Sha, R.; Birktoft, J. J.; Hernandez, C.; Mao, C.; Seeman, N. C. *Nat. Chem.* **2017**, *9* (8), 824.
(35) Seeman, N. C. *J. Theor. Biol.* **1982**, *99* (2), 237−247.
(36) Fu, T. J.; Seeman, N. C. *Biochemistry* **1993**, *32* (13), 3211−3220.
(37) Hong, F.; Jiang, S.; Wang, T.; Liu, Y.; Yan, H. *Angew. Chem.* **2016**, *128* (41), 13024−13027.
(38) Ouldridge, T. E.; Louis, A. A.; Doye, J. P. *J. Chem. Phys.* **2011**, *134* (8), 085101.
(39) Srinivas, N.; Ouldridge, T. E.; Šulc, P.; Schaeffer, J. M.; Yurke, B.; Louis, A. A.; Doye, J. P.; Winfree, E. *Nucleic Acids Res.* **2013**, *41* (22), 10641−10658.
(40) Rothemund, P. W.; Ekani-Nkodo, A.; Papadakis, N.; Kumar, A.; Fygenson, D. K.; Winfree, E. *J. Am. Chem. Soc.* **2004**, *126* (50), 16344−16352.
(41) Sun, X.; Hyeon Ko, S.; Zhang, C.; Ribbe, A. E.; Mao, C. *J. Am. Chem. Soc.* **2009**, *131* (37), 13248−13249.
(42) Aghebat Rafat, A.; Pirzer, T.; Scheible, M. B.; Kostina, A.; Simmel, F. C. *Angew. Chem., Int. Ed.* **2014**, *53* (29), 7665−7668.
(43) Suzuki, Y.; Endo, M.; Sugiyama, H. *Nat. Commun.* **2015**, *6*, 8025.
(44) Kocabey, S.; Kempter, S.; List, J.; Xing, Y.; Bae, W.; Schiffels, D.; Shih, W. M.; Simmel, F. C.; Liedl, T. *ACS Nano* **2015**, *9* (4), 3530−3539.
(45) Avakyan, N.; Conway, J. W.; Sleiman, H. F. *J. Am. Chem. Soc.* **2017**, *139* (34), 12027−12034.
(46) Lan, X.; Chen, Z.; Dai, G.; Lu, X.; Ni, W.; Wang, Q. *J. Am. Chem. Soc.* **2013**, *135* (31), 11441−11444.
(47) Kuzyk, A.; Schreiber, R.; Zhang, H.; Govorov, A. O.; Liedl, T.; Liu, N. *Nat. Mater.* **2014**, *13* (9), 862.

DOI: 10.1021/jacs.8b07180
J. Am. Chem. Soc. 2018, 140, 14670−14676